Materials Today Communications 35 (2023) 105653

Contents lists available at ScienceDirect

Materials Today Communications

journal homepage: www.elsevier.com/locate/mtcomm

High power asymmetric supercapacitor based on activated carbon/reduced graphene oxide electrode system

Nomxolisi Dywili [a,b], Afroditi Ntziouni [b], Miranda M. Ndipingwi [a], Chinwe Ikpo [a], Assumpta C. Nwanya [a,c,*], Konstantinos Kordatos [b,**], Emmanuel Iwuoha [a,**]

[a] SensorLab, University of the Western Cape Sensor Laboratories, Chemical Sciences Building, Robert Sobukwe Road, Bellville, Cape Town 7535, South Africa
[b] National Technical University of Athens, School of Chemical Engineering, Section I: Chemical Sciences, Labs of Inorganic and Analytical Chemistry, 9 Heroon Polytechniou Str., Athens 15773, Greece
[c] Department of Physics and Astronomy, University of Nigeria, Nsukka

ARTICLE INFO

Keywords:
Energy storage
Graphene
Graphene oxide
Reduced graphene oxide
Supercapacitor

ABSTRACT

We synthesized Graphene oxide (GO) using the modified Hummers method and further reduced to reduced graphene oxide (rGO) using hydrazine monohydrate and ammonia solution. The prepared materials were interrogated using different characterization techniques to determine which of them is more suitable for supercapacitor application. High resolution scanning electron microscopy (HRSEM) revealed a sheet-like morphology of separated thin sheets and wrinkled edges for GO, whereas rGO consist of thinner sheets with smaller pores than GO. The structural studies as elucidated from X-ray diffraction (XRD) shows that the GO has more interlayer spacing due to a higher oxygen content as compared to the rGO. The oxygen containing functional groups seen in GO either disappear or are greatly reduced in intensity in rGO as evidenced from the Fourier transform infrared spectroscopy (FTIR) of the materials. The electrochemical studies indicate that the rGO gave a higher current response compared to GO and a specific capacitance of 105.3 and 56.7 F g^{-1} respectively was delivered by rGO and GO at a scan rate of 10 mV s^{-1} in a three-electrode set-up. Asymmetric supercapacitor cells using GO and rGO as positive electrodes and activated carbon as the negative electrodes gave the highest specific capacitance value of 94.3 F g^{-1} for the AC//rGO cell and 59.6 F g^{-1} for the AC//GO cell at a current load of 0.25 A g^{-1}. The specific capacitance obtained from the AC//rGO is comparable to most recorded values for rGO electrodes. A high specific power of 6411.7 W kg^{-1} was obtained at a specific energy of 22.6 W h kg^{-1} while at a specific energy of 25.7 W h kg^{-1}, a specific power of 700.1 W kg^{-1} was obtained for the AC//rGO. This is due to the more porous and thinner sheet of the rGO. The overall results showed that the rGO gave better supercapacitive properties than the GO.

1. Introduction

The energy challenges brought by increased population growth and the concomitant increase in the energy requirements of modern society, global warming and unfolding ecological concerns has made it pertinent that new, cost effective, flexible and environmentally benign energy storage systems be developed [1]. Supercapacitors are energy storage devices with very high power and moderate energy densities with low inner resistance that can accumulate and supply energy at comparatively higher capacities when in comparison to batteries. This is because the technique of energy storage involves a simple charge separation at the electrode-electrolyte interface [2,3]. The advantages of supercapacitors when compared with other energy storage devices include but are not limited to extended life, elevated power, pliable packaging, extensive stable thermal range (−40 to 70 °C), little maintenance cost and low weight [4]. However, supercapacitors are challenged with small energy density, low voltage per cell as well as elevated self-discharge.

The active material of an electrode is appraised as one of the most salient components of supercapacitors. Developing new electrode materials to overcome the obstacle of low energy has become paramount

* Corresponding author at: SensorLab, University of the Western Cape Sensor Laboratories, Chemical Sciences Building, Robert Sobukwe Road, Bellville, Cape Town 7535, South Africa.
** Corresponding authors.
E-mail addresses: chinwe.nwanya@unn.edu.ng (A.C. Nwanya), kodartos@central.ntua.gr (K. Kordatos), eiwuoha@uwc.ac.za (E. Iwuoha).

https://doi.org/10.1016/j.mtcomm.2023.105653
Received 9 November 2022; Received in revised form 30 January 2023; Accepted 15 February 2023
Available online 22 February 2023
2352-4928/© 2023 Elsevier Ltd. All rights reserved.

[5]. The most promising materials for supercapacitors today are carbon materials (carbon nanotubes, carbon black, graphene, carbon aerogels, and activated carbon and carbon ink), metal oxides, conducting polymers and a combination of each which gives a composite [6,7]. Carbon materials are used due to high specific areas, lower cost, and more developed and traditional fabrication techniques in comparison to other materials [8,9]. Metal oxides are used because of their higher derivable specific capacitance in addition to their low resistance making them facile for high energy and power supercapacitors. Conducting polymers use the mechanism of redox reactions to store and release charge [10–13]. Currently, researchers' focus is on the development of techniques to enhance the energy density while sustaining the intrinsic high power density and fast charge/discharge for supercapacitors [14].

Graphene and graphene oxide have recently received rapidly growing attention in supercapacitor applications due to their exceptional properties. Graphene is a single layer of graphite and promises to be a good supercapacitor material due to its intrinsic properties. It possesses a large theoretical specific surface area of 2600–2675 $m^2\ g^{-1}$, high intrinsic mobility of 200 000 $cm^2\ V^{-1}\ s^{-1}$, elevated Young's modulus ~ 1.0 Pa, thermal conductivity of ~ 5000 $Wm^{-1}\ K^{-1}$, optical transmittance of ~ 97.7% and outstanding electrical conductivity [9, 15]. These properties deserve attention for transparent conductive electrode applications [15]. In view of the agglomeration of graphene nanosheets, the practical surface area of graphene is usually much reduced than the theoretical one and its derivable specific capacitance is largely in the range of 100–200 F g^{-1} [16]. Graphene oxide (GO), a lone sheet of graphite oxide is one of graphene's derivatives. It consists of a large range of reactive oxygen functional groups [17]. The atomic sheets of GO usually involves phenol epoxy and epoxide groups on the basic plane and easily ionizing carboxylic acid groups all over the edges. It has superior electrical, enhanced mechanical strength, stable thermal properties and elevated surface area which makes it amenable for use in polymer composites, as energy-related materials, in sensors, as 'paper'-like materials, in field-effect transistors (FET) and in biomedical applications [18]. GO is advantageous due to its easy dispersibility in water and other organic solvents as well as in other matrixes [19]. This advantage derives from the presence of the oxygen functionalities. GO is hydrophilic due to its polar functional groups. It is well dispersible in water and can be exfoliated in many solvents. Dispersions of GO flakes can be produced by stirring and more commonly by ultrasonicating of GO in solvents [20].

The colloidal dispersions of GO are chemically reduced by various reducing agents such as hydrazine, hydroquinone, sodium borohydride and ascorbic acid [21] to get reduced graphene oxide (rGO). Other methods of reduction such as reduction via thermal treatment and electrochemical reduction are also considered to be very effective [22]. Reduction via thermal treatment has not only been reported to be efficient and cost effective but produces material with high BET surface area in the range of 600–900 $m^2\ g^{-1}$ [23]. Electrochemical reduction has been reported as an effective method to get rid of the oxygen functionalities of GO [24]. The exfoliation of graphite into GO by chemical procedure, accompanied by tractable reduction of GO (with reducing agents such as hydrazine hydrate) into rGO is considered and taken to be one of the most efficient and cost effective methods [27,28] and the schematic is as shown in Fig. 1. Though individual rGO sheets are in many instances agglomerated to a limited extent into particles whose diameters are approximately in the range of 15–25 μm during the reduction process, products with enhanced specific surface areas of up to a few hundred m^2g^{-1} can be achieved. The rGO sheets are therefore, potential electrode materials for efficient energy storage device applications [27].

There have been some contentions in the literature between GO and rGO which constitute a better electrode to be used in supercapacitors. While some authors show that GO is better in terms of the specific capacitance obtained, others indicate that rGO is better especially if the electrical conductivity and stability is of importance [28,29]. Gao and Georgalilas et al., observed that GO possesses less stacking stability and poor conductivity, therefore when used alone as a carbon material, it does not serve as a superior electrode material for supercapacitors [25, 30]. Based on the value of the specific capacitance obtained by Xu et al., they were of the opinion that GO may be a better electrode material than graphene for supercapacitors [31]. However, Rai et al., [32] showed that because the lattice spacing in rGO is reduced due to the removal of the oxygen-based functional groups, defect density and the number of stacking in rGO is reduced and this resulted to an increase in the specific capacitance of rGO in comparison to GO. Yang et al., also observed that reduction modification of GO is needed to optimize its electrochemical performance [33]. Therefore, it is necessary to properly investigate which one to use between GO and rGO in the construction of electrodes for supercapacitors. Hence in this paper, we determined which is more proper to use in supercapacitors; GO or rGO.

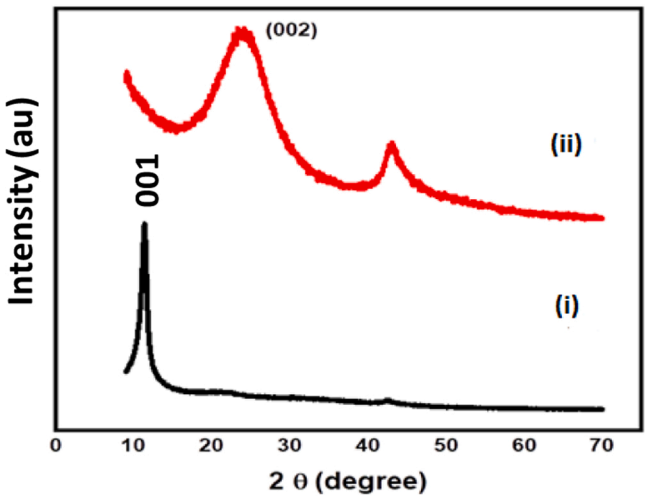

Fig. 1. XRD patterns of (i) GO and (ii) rGO.

2. Experimental details

2.1. Chemicals and sample preparation

Analytical grade chemicals were utilized as procured with no additional purification process. Graphite (1–2 μm), hydrochloric acid (HCl) (≥37%), sodium nitrate ($NaNO_3$), sulphuric acid (H_2SO_4) (≥ 98%), potassium permanganate ($KMnO_4$) (≥ 99%), hydrogen peroxide (≥ 30%), acetone (≥99.9%) and hydrazine monohydrate, reagent grade (98%) were all procured from Sigma-Aldrich, Cape Town, South Africa.

2.2. Synthesis of GO and rGO

Graphene oxide (GO) was prepared utilizing a modified Hummers method. The details of the procedure is contained in our previous work [34]. The prepared GO was reduced to rGO by using hydrazine monohydrate as the reducing agent. 100 mg of GO was diffused in 200 mL of deionized water and ultra-sonicated for three hours by which the bulk GO powders were modified into GO sheets. The obtained brown precipitation/dispersion was centrifuged at 3000 rpm for 30 min to get rid of any excess un-exfoliated GO. A volume of 200 μL of hydrazine monohydrate and 3 mL of ammonia solution were then added to the solution of GO. The mixture was stirred energetically for 10–20 min and refluxed at 80 °C overnight in an oil bath. The final product was then centrifuged or filtered, washed with deionized water and dehydrated under vacuum overnight [35,36].

2.3. Characterizations of the GO and rGO

We used Nicolet Evolution 100 UV-Visible spectrophotometer (Thermo Electron, UK) to measure the absorption characteristics of the prepared GO and rGO over a wavelength range of 200–800 nm. Fourier transform infrared (FTIR) spectra showing the functional groups and bonds in the materials were recorded on a Perkin Elmer FTIR model 100 spectrophotometer, between 400 and 4000 cm^{-1}. The high-resolution scanning electron microscopy micrographs (HRSEM) of GO and rGO were imaged using a Ziess Auriga SEM operating at 50 kV. The crystal structures of the samples were ascertained from the x-ray diffraction patterns gotten from a D8 Advanced diffractometer manufactured by Bruker AXS in Germany. Raman spectroscopy was taken with a Renishaw Invia Raman Microscope made in Germany and a Class 1 Laser product was used. Electrochemical measurements were obtained in both three and two-electrode cells on a VMP-300 potentiostat from Bio-Logic instruments (Knoxville, TN, USA).

2.4. Fabrication of the electrode

The electrodes were developed by blending the active materials in a mortar with a conductive agent (carbon black) and a binder (polytetrafluoroethylene) in the ratio 7:2:1 utilizing a little quantity of anhydrous N-methyl-2-pyrrolidone to obtain a homogeneous paste. 0.5×1 cm^2 dimension of nickel foam as well as 20 mm diameter of coin-shaped ones were cut and ultrasonicated in 1 M solution of HCl for 15 min to remove any surface oxide layer that may be present. The nickel foam substrates were further rinsed by ultrasonication in absolute ethanol and deionised water separately for 15 min each and finally dehydrated at 90 °C for 12 h. The electrode paste was deposited on the nickel foam substrates using a spatula and then dried at 80 °C for 12 h. Ag/AgCl served as the reference while Pt wire was used as the counter electrode, in a three-electrode study of the electrode materials. For two-electrode cell analysis, the homogenous paste was deposited on the 20 mm diameter coin-shaped nickel foam and assembled in a Swagelok using the nanosheets of GO and rGO as the positive electrodes while activated carbon served as the negative electrode. Cyclic voltammetric (CV) curves were obtained in a potential range of − 0.3–0.3 V at various scan rates while the electrochemical impedance measurements were acquired at a frequency range of 0.1 MHz −100 kHz at room temperature. Cyclic voltammetric experiments, galvanostatic charge-discharge (GCD) curves and the cycling performance of the supercapacitor cells were all acquired in 1 M KOH electrolyte at a voltage of 1.4 V.

The specific capacitance (F g^{-1}) of the GO and rGO electrode materials was calculated from the CV and GCD curves for a 3-electrode cells according to Eqs. (1) and (2), respectively.

$$C_{sp} = \frac{1}{2m\upsilon V}\int_{-v}^{+v} Idv \tag{1}$$

$$C_{sp} = \frac{Ixt}{m\left(V - IR_{drop}\right)} \tag{2}$$

where m, υ, and V, denotes the active mass of the electrode (g), the scan rate (V s^{-1}), and the potential window (V) respectively. $\int_{-V}^{+V} Idv$ is the total charge (A s) for the electrochemical reaction, obtained by integrating the positive and negative CV curves, IR_{drop} is the voltage drop/equivalent series resistance (V), I depicts the applied current (A) and t denotes the charge/discharge time (s).

The specific capacitance (F g^{-1}) of GO and rGO based supercapacitor (2-electrode) cells was calculated from GCD curves using Eq. 3.

$$C_{sp} = \frac{4Ixt}{mV} \tag{3}$$

where m is the entire mass of both the positive and negative electrodes (g), V is the highest voltage, while other parameters are as described above.

The specific energy in W h kg^{-1} and specific power in W kg^{-1} of the supercapacitor cells at various current densities were calculated using Eqs. 4 and 5 respectively.

$$E = 1/2C_{sp}x\Delta V^2x1/36 \tag{4}$$

$$P = E/\Delta tx3600 \tag{5}$$

where C_{sp} depicts the specific capacitance (F g^{-1}), ΔV is the applied potential (V), and Δt is the discharge time (s).

3. Results and discussion

3.1. Structural properties of GO and rGO

Fig. 1(i) shows the XRD patterns of GO, revealing a very sharp diffraction peak (001) appearing at $2\theta = 11.08°$ with a d spacing of 0.905 nm. This peak indicates that AB stacking exists in GO with larger interlaying spacing as compared to graphite (0.336 nm) due to the presence of oxygen containing functional groups in the layers [37,38]. The position of this diffraction peak is a function of the preparation method as well as the number of layers of water in the interplanar space of the material. The GO was reduced in the presence of hydrazine monohydrate to obtain rGO and the XRD pattern (Fig. 1 (ii)) shows a broad peak centred around at 25.5° due to (002) reflection of the rGO and having a d spacing of 0.36 nm. This band is very broad indicating the poorly ordered free graphene nanosheets and that significant portion of GO has been greatly reduced [39]. Furthermore, the broad nature of the reflection in rGO indicates poor orderly arrangement of the sheets along the stacking direction [26]. This implies that the rGO could have been entirely exfoliated to consist mostly of a single layer, a few layers and/or even loosely stacked layers [40].

Fig. 2 displays the FTIR spectra of GO (i) and shows the vibrational bands of O-H stretching vibrations at 3431 cm^{-1}, C═O (carboxylic acid and carbonyl moieties) at 1731 cm^{-1} and the graphitic domains of C═C at 1644 cm^{-1} and O═C-O at 1394 cm^{-1}. The band from 980 – 1250 cm^{-1} consists of the C–O (1059 cm^{-1}) and the CO–H (1227 cm^{-1}) deformation, respectively, of carboxylic acid groups [20], [41][42]. The characteristic bands of GO's functional groups confirm the oxidation of graphite [42]. The band found around 1644 cm^{-1} results from the vibration of the aromatic C═C bond of the sp^2 unoxidized network [43,44]. The FTIR spectrum of rGO (Fig. 2ii) reveals that the oxygen bands either disappear or are greatly reduced in intensity while a new peak that appears at 656 cm^{-1} is attributed to C-C bonds that are

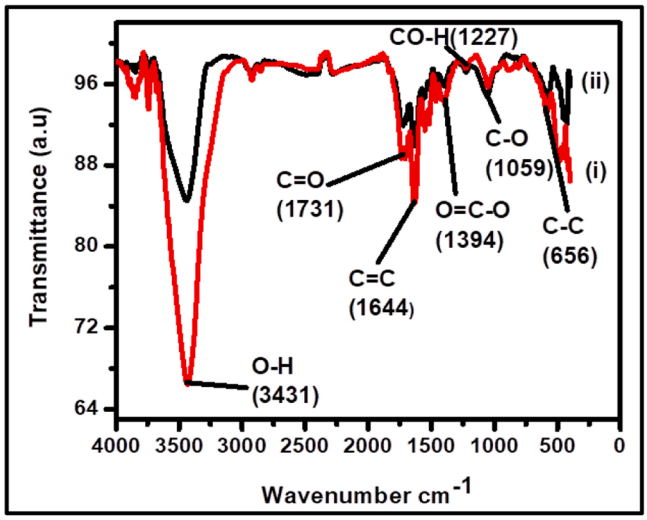

Fig. 2. FTIR spectra of GO (i) and rGO (ii).

due to thermal annealing [45]. The hydroxyl group was also drastically reduced in the rGO, hence the chemical reduction process could serve as an effective means to remove the hydroxyl functionalities [38].

Raman spectroscopy was used to elucidate the internal structural properties of the GO and rGO. The technique is used widely to analyze carbon based materials, because conjugated and C═C bonds result to elevated Raman intensities [46]. In GO and rGO, the Stokes phonon energy shift originated by laser excitation produces two main bands (D and G) in the Raman spectrum [42]. GO (Fig. 3.) shows a D band (1347 cm^{-1}); a second-order overtone of a dissimilar in-plane vibration that correlates to defects within the sp^2 network, a G band (1595 cm^{-1}) and a 2D band (2679 cm^{-1}) attributed to primary in-plane vibrational mode [47,48]. In rGO (Fig. 3.), the D band and G band are shifted to higher frequencies due to the incomplete defect healing and because of additional forces from the interplay between the layers of AB-stacked graphene that increases the graphitic domain compared to GO. The spectrum changes from that of single-layer graphene as the number of rGO layers increases, [49]. This therefore splits the 2D band into more number of modes that can merge resulting to a broader, smaller intensity but elevated frequency band [50]. The G band increased while the D band reduced in the rGO and this indicates the increase in the sp^2 graphitic domain and the reduction of defects respectively in rGO as compared to GO. The ratio of *ID/IG* is higher in GO and indicates higher order. The number of layers are derived from the band intensities *IG/I2D* ratio in addition to the position and shape of these bands for the AB-stacked rGO [51]. The graphene layers (as calculated from the ratio of *IG/I2D*) reduced while the in-plane crystallite size (calculated from *La* (*nm*)= 4.4*IG/ID*) increased (Table 1). These showed that the layers reduced while and the in-layer crystallite sizes increased indicating the successful reduction of GO to rGO.

3.1.1. Morphological properties of GO and rGO

High-resolution scanning electron microscopy (HRSEM) was used to determine surface morphology of the GO and rGO materials. Both the GO and rGO were efficiently exfoliated into separated thin sheets and wrinkled to form porous structures as shown in Fig. 4(a) and (b) [42]. HRSEM image of GO shows an absorbent network that resembles a loose sponge like structure due to the well-defined and interlinked three-dimensional graphene sheets, [31,52]. In comparison, the rGO consists of thinner sheets and smaller pores than GO as was also reported by Drewniak et al., [53]. The GO nanosheets exhibit to some extent the stacking structure with a sheet-like morphology of large thickness, smooth surfaces and wrinkled edges in agreement with earlier reports [35,54,55] while rGO shows thin layered structure of minimum sheet thickness [56]. This is further corroborated in the side view shown in Fig. 4c and d for GO and rGO respectively.

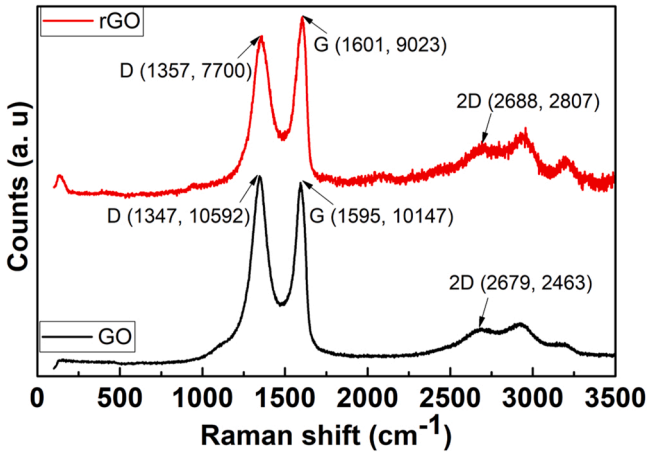

Fig. 3. Raman spectroscopy of GO and rGO.

Table 1
The bands and the respective Raman Shifts in GO and rGO.

Material	Band	Raman Shift		*ID/IG*	*IG/2D*	*La (nm) = 4.4 IG/ID*
		Position (cm^{-1})	Intensity I			
GO	D	1346.98	10591.55	1.04	4.12	4.22
	G	1594.69	10147.29			
	2D	2678.64	2462.66			
rGO	D	1356.59	7699.77	0.85	3.52	5.65
	G	1601.74	9022.63			
	2D	2687.98	2806.73			

The TEM images as shown in Fig. 5 indicates that the GO nanosheets are flat with some wrinkles and the bends were due to the numerous defects and functional groups of sp^3 hybridized carbon atoms during the oxidation process (Bhattacharya et al., 2017). In general, GO nanosheets tend to be assembled with each other and forms multilayer agglomerates. The rGO appears with less wrinkles compared to the GO.

3.1.2. Optical properties of GO and rGO

GO has unique optical properties that can be integrated to different applications. UV-Vis spectra of aqueous GO solutions are shown in Fig. 6 (i) at increasingly concentrated aqueous solutions. Two types of typical features were distinguished in these spectra to identify GO. The first is a shoulder band at ~311 nm, which corresponds to an n-π * plasmon band. The shoulder bands observed for all the samples are similar. Another typical feature appears at 227 nm, and is related to a π-π * plasmon band [57,58]. From the UV-Vis spectroscopic studies, it can be deduced that the optical absorption of GO is dominated by the π-π * plasmon band near 227 nm [59]. The π-π * plasmon band depends on nanometer-scale sp^2 clusters and from linking chromophore units such as C═C, C═O and C–O bonds [20,60].

The UV-Vis spectrum of rGO (Fig. 6 ii) shows a typical band at 264 nm, demonstrating the restoration of the extensive conjugated sp^2 carbon network [61,62]. The absorption band shifts to lower absorption wavelengths due to the reduction of oxygen functional groups and an enhancement in the aromatic rings leading to easy excitation of electrons to a lower frequency [63].

3.2. Electrochemical properties of GO and rGO

3.2.1. Cyclic voltammetric (CV) studies

CV curves were obtained at scan rates of 10 – 150 mV s^{-1} at a potential window of − 0.3–0.3 V. The CV curves displayed near rectangular-shaped voltammograms as shown in Fig. 7(a), with a minimum change in shape, indicating good capacitive behavior. Fig. 7(a) shows the CV profiles of GO and rGO compared at 20 mVs^{-1}. rGO exhibits a higher current response over GO, depicting better charge propagation due to less agglomeration of the rGO nanosheets and faster diffusion of ions within the structure. The specific capacitance values of GO and rGO calculated from the CV curves using Eq. 1 are plotted in Fig. 7(c). rGO delivered a specific capacitance of 105.3 F g^{-1} at 10 mV s^{-1}, which decreased to 15.6 F g^{-1} at 150 mV s^{-1}, while GO showed a specific capacitance of 56.7 F g^{-1} at 10 mV s^{-1}, which also decreased to 12.4 F g^{-1} at 150 mV s^{-1}. The decrease in the specific capacitance with increasing scan rate can be attributed to a diffusion-controlled charge storage mechanism, whereby at lower scan rates, the electrolyte has enough time to go through the electrode pores resulting to a higher specific capacitance [64]. Contrariwise, movement of ions at the electrode-electrolyte interface is faster at higher scan rates, resulting in only the outer surface of electrode material being in contact with the electrolyte.

3.2.2. Galvanostatic charge-discharge (GCD) studies

GCD curves of GO and rGO nanosheets are shown in Fig. 8. The rGO

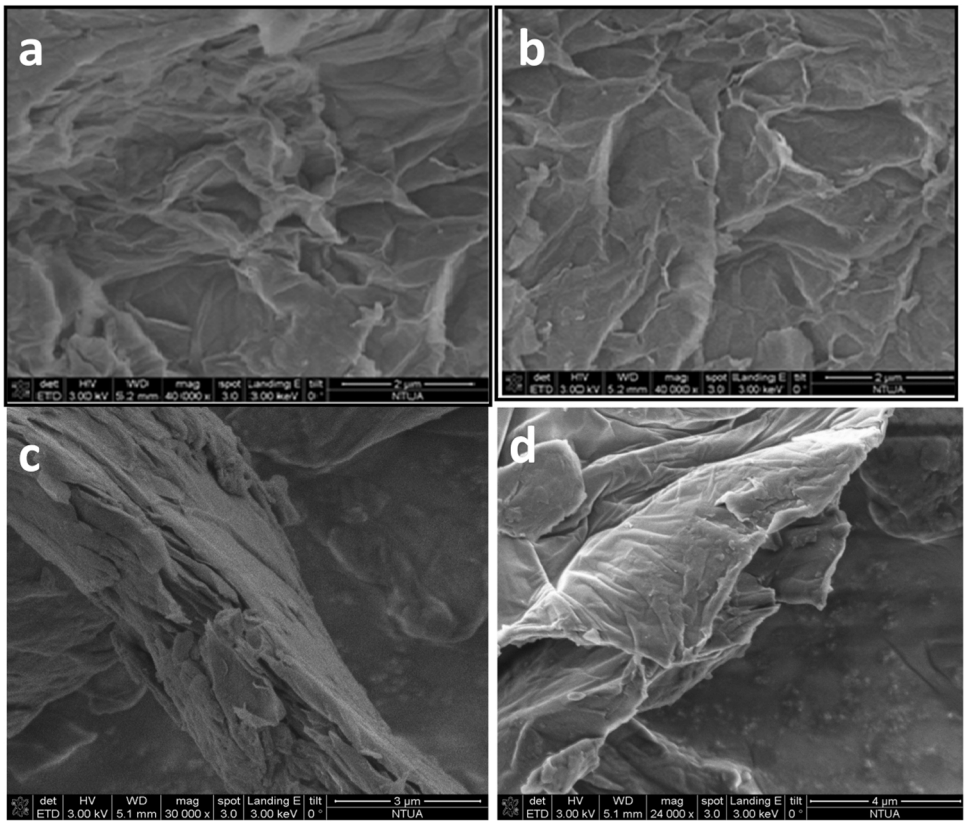

Fig. 4. : HR-SEM micrographs of (a) GO at 2 μm (b) rGO at 2 μm; cross section of the SEM Images (c) GO and (d) rGO.

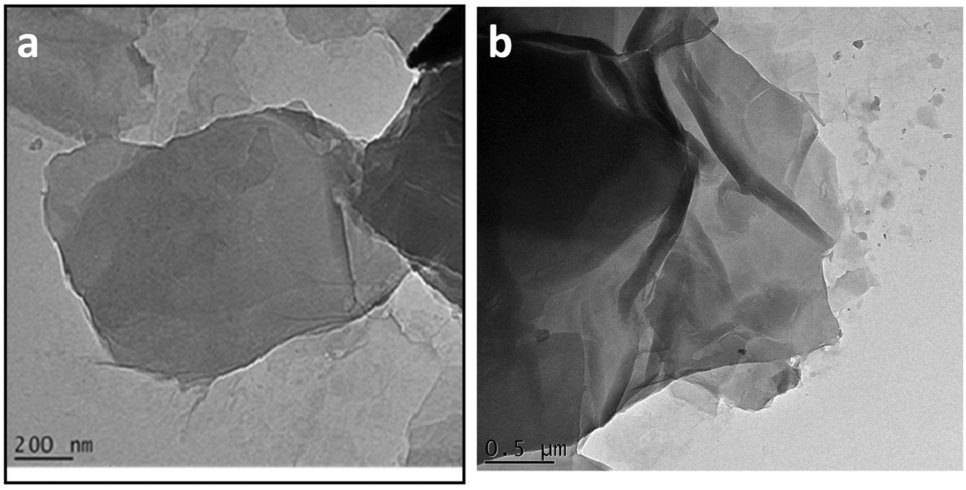

Fig. 5. TEM images of (a) GO, (b) rGO.

nanosheets presented almost linear GCD profiles with a small IR drop, indicating a fast current-voltage response. The specific capacitance values obtained from the GCD curves according to Eq. 2 are displayed in Fig. 8(c). rGO nanosheets delivered a specific capacitance of 69.1 F g^{-1} at 0.75 A g^{-1}, which is about twofolds higher than the C_{sp} of GO (32.47 F g^{-1}) obtained at 0.75 A g^{-1}. This could be associated with more porous and thinner rGO nanosheets structures observed in HRSEM studies, which facilitated the ion diffusion within the host material [65].

3.3. Electrochemical impedance spectroscopic (EIS) studies

EIS was used to probe the interfacial properties of GO and rGO electrode materials. The EIS data was recorded at open circuit voltage at a frequency range of 0.1 MHz to 100 kHz at 6 points per decade. The Nyquist and Bode plots of GO and rGO electrode materials are displayed in Fig. 9(a) and (b), respectively. The Nyquist plots consist of semicircles at the high frequency region, which represent the charge transfer resistance (R_{ct}) and an inclined line in the mid to low frequency region associated with the Warburg diffusion (W_o) within the electrode materials. The circuit model used to fit the EIS plots using Zview is displayed as the inset in Fig. 9(a). The internal resistance and wettability of the materials (R_s) is obtained from the intercept of the semicircle on the X-axis. As shown in Table 2, R_s is observed to decrease from GO to rGO, indicating the improved wettability and lower internal resistance of rGO

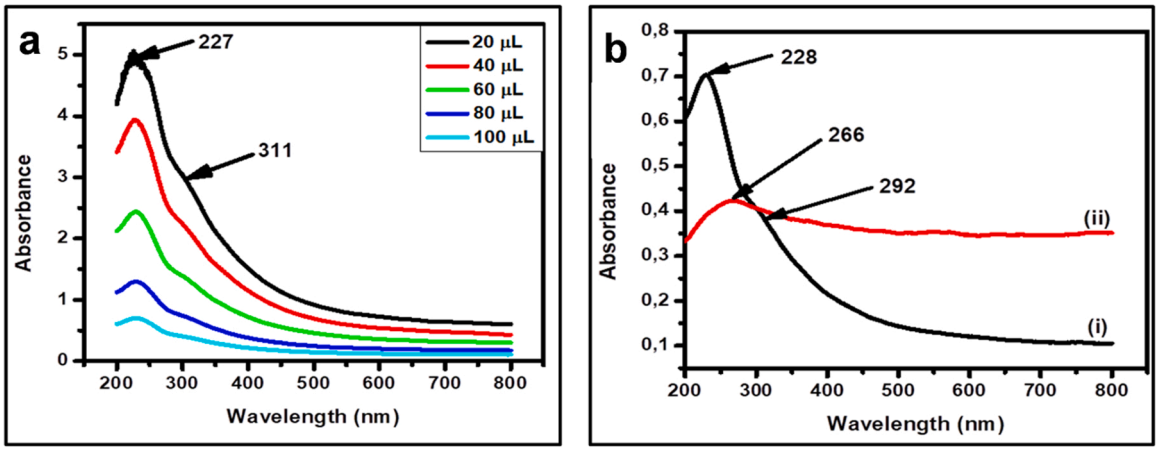

Fig. 6. : UV-Visible spectra (200–800 nm wavelength region) in de-ionized water of (a) GO from increasingly concentrated aqueous solutions, 20, 40, 60, 80 and 100 µL in in de-ionized water (b) (i) GO and (ii) rGO at concentration of 20 µL.

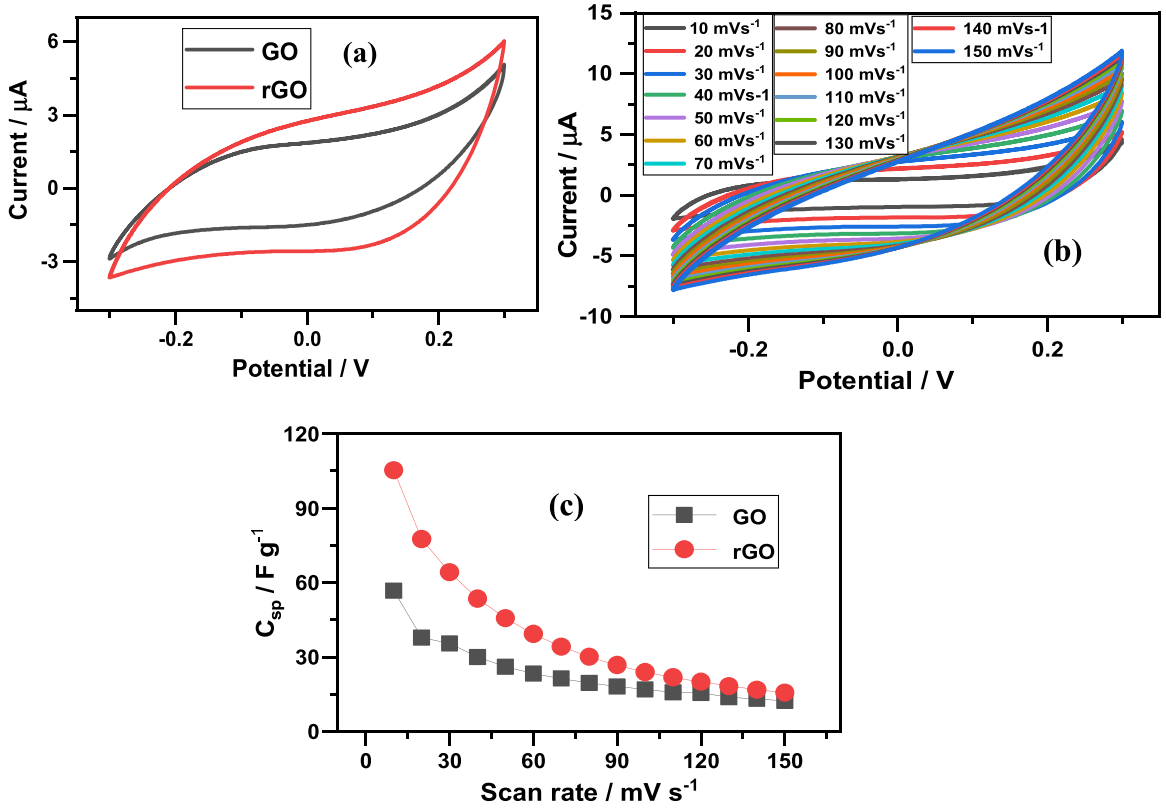

Fig. 7. CV curves of GO and rGO at 20 mVs^{-1} (a), CV curves of rGO at scan rates of 10 – 150 mVs^{-1} (b) and Variation of the specific capacitance with scan rate of Go and rGO (c).

[66]. rGO showed a smaller semicircle with a lower charge transfer resistance of 15.04 Ω compared to 22.88 Ω for the GO electrode, indicating better charge mobility in rGO than in GO. A lower Warburg component in rGO (0.36 Ω) over GO (0.41 Ω) also suggests shorter ion diffusion pathways in the latter than in the former [67].

3.4. Electrochemical performance of GO and rGO as supercapacitor electrodes

The potential application of GO and rGO in supercapacitors was investigated by assembling asymmetric supercapacitors cells using GO and rGO as positive electrodes and activated carbon as the negative electrode. To maximize the performance of the supercapacitor cells, the mass loading of the positive and negative electrodes was adjusted according to the mass-charge balance equation, Eq. 6 below [69].

$$\frac{M^{+}}{M^{-}} = \left(\frac{C^{-}_{sp} x \Delta V^{-}}{C^{+}_{sp} x \Delta V^{+}}\right) \tag{6}$$

The total mass of the AC//rGO supercapacitor cell was adjusted to 6.09 mg. The mass of the positive electrode was at 3.20 mg while the mass of the negative electrode was at 2.89 mg. Similarly, the total mass of the AC//GO cell was 7.77 mg, with 5.12 mg for the positive electrode and 2.51 for the negative electrode.

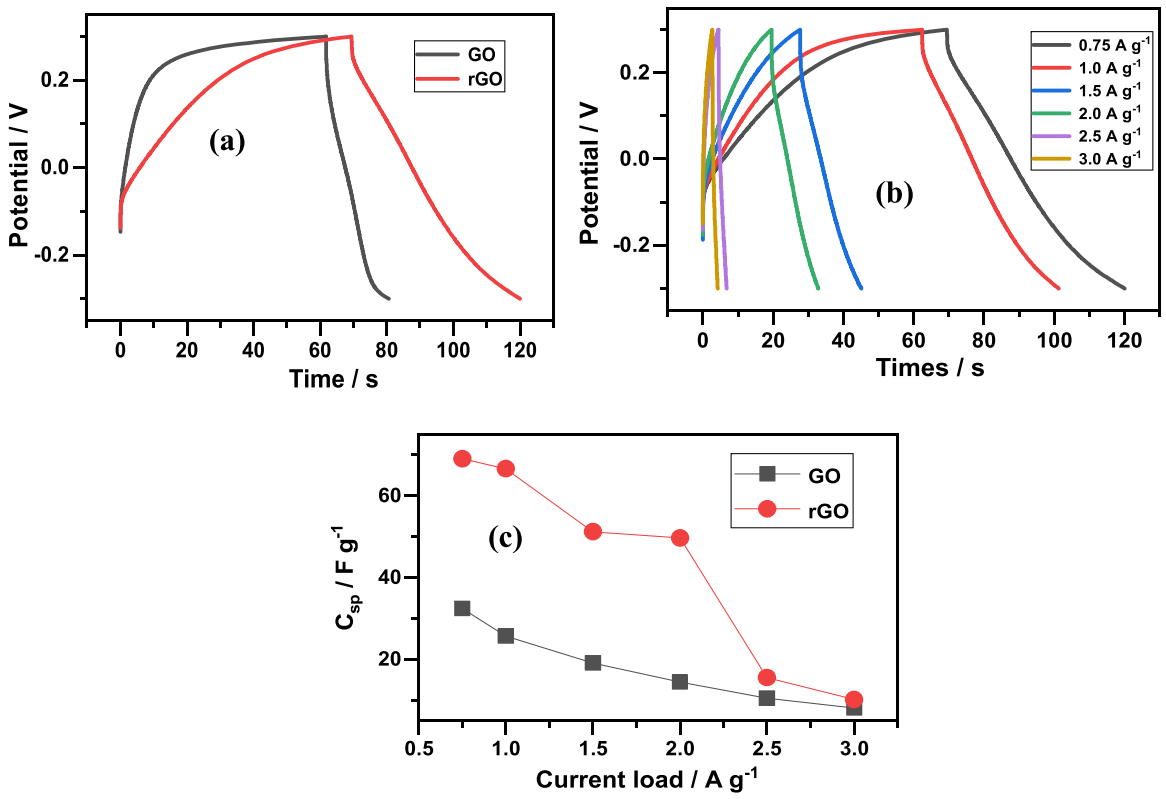

Fig. 8. GCD curves of GO and rGO at 0.75 A g^{-1} (a), GCD profiles of rGO at different current loads (b), Variation of the specific capacitance with current load of GO and rGO (c).

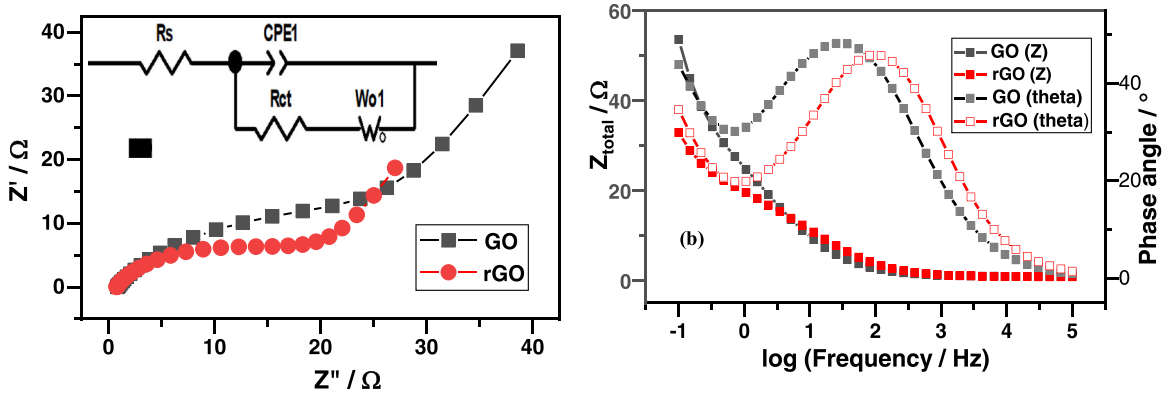

Fig. 9. Nyquist plots of GO and rGO (a) and the equivalent circuit used for curve fitting as the inset. Bode plots of GO and rGO (b).

Table 2
EIS data obtained from curve fitting the plots using Zview.

Electrode material	R_s / Ω	CPE/ μF	R_{ct} / Ω	Wo /Ω $s^{-1/2}$	Phase angle /°
GO	0.84	0.73	22.88	0.41	52.8
rGO	0,76	0.75	15.04	0.36	51.2

3.4.1. *Galvanostatic charge discharge studies*

Fig. 10 (a) and (b) shows the GCD curves of GO and rGO based supercapacitor cells with activated carbon in 1 M KOH at a voltage window of 1.4 V. The AC//GO and AC//rGO supercapacitor cells displayed almost linear GCD profiles, which were also observed in the three electrode characterizations. Fig. 10 (c) displays the variation of the specific capacitance values obtained from the GCD curves with the various current load. A maximum value of 94.3 F g^{-1} for the AC//rGO cell and 59.6 F g^{-1} for the AC//GO cell were obtained at a current load of 0.25 A g^{-1}. It was observed that the specific capacitance of both supercapacitor cells decreased as the current load increased. This can be ascribed to lower ionic migration into the electrode surface at higher current loads.

3.4.2. *Cycling stability*

The stability of the GO and rGO based supercapacitor cells was tested at a voltage window of 0 – 1.4 V over 5000 GCD cycles. Fig. 11 (a) shows the retention capability of the specific capacitance of AC//GO and AC//rGO supercapacitor cells after 5000 cycles at a current load of 0.75 Ag^{-1}. The AC//rGO cell maintained a good capacitance of 73.5% and an excellent coulombic efficiency of 99.8% (Fig. 11 (b)) over 5000 cycles. While the AC//rGO cell exhibited a capacitance retention of 54.4% and a coulombic efficiency of 99.3%. The excellent coulombic efficiency of both the AC//rGO and AC//GO cells demonstrates the good reversibility

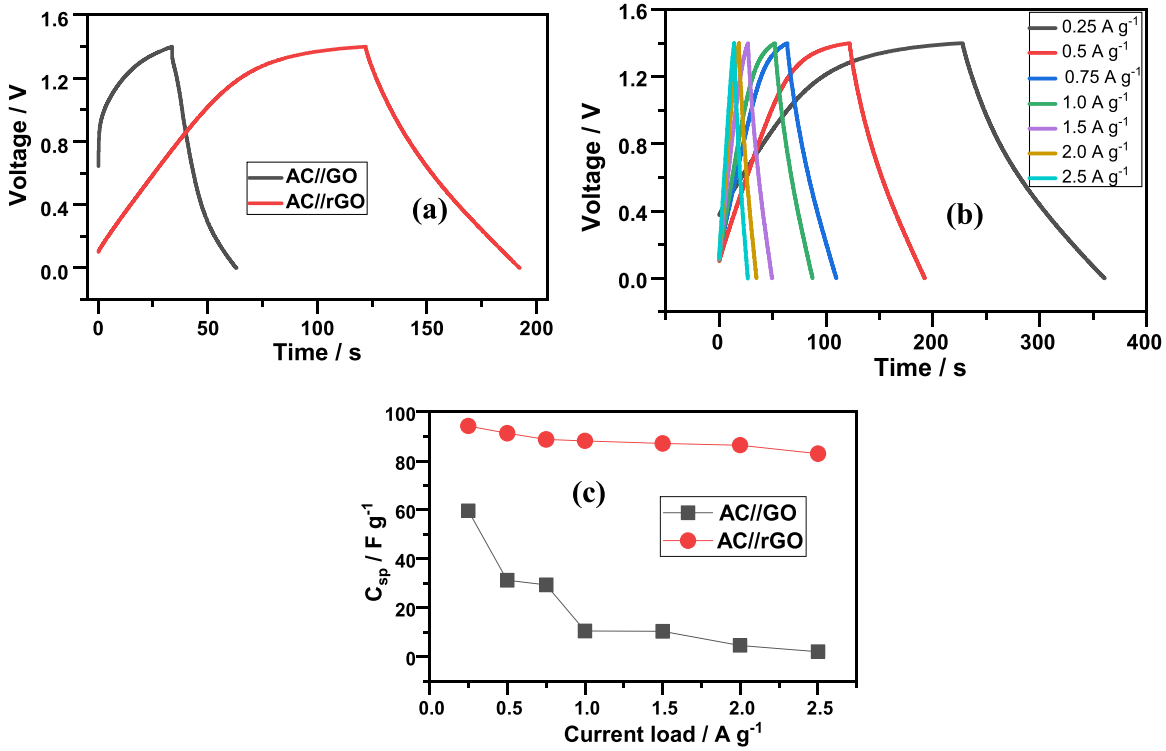

Fig. 10. GCD curves of AC//GO and AC//rGO at 0.5 A g^{-1} (a), GCD profiles of AC//rGO at various current loads (b), Variation of the specific capacitance with current load of AC//GO and AC//rGO (c).

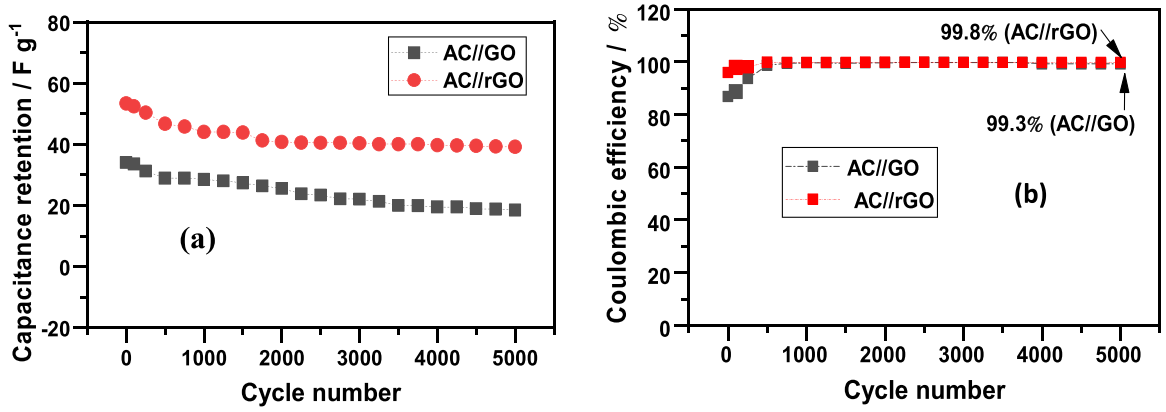

Fig. 11. Cycling stability (a) and Coulombic efficiency (b) of AC//GO and AC// rGO supercapacitor cells over 5000 cycles.

of the supercapacitor devices. The initial decrease in capacitance may be ascribed to the preliminary change of functional groups on the conjugated carbon backbone as electrolyte ions are adsorbed into the pores during the repeated charge discharge process [68].

3.4.3. *Specific energy and specific power*

The practical energy storage application of the AC//GO and AC// rGO cells is presented in the Ragone plot (Fig. 12). The specific energy and specific power of the cells were calculated according to Eqs. 4 and 5 [69,70]. The AC//rGO supercapacitor cell achieved a specific energy of 25.7 W h kg^{-1} at a specific power of 700.1 W kg^{-1} and was able to retain a specific energy of 22.6 W h kg^{-1} at a specific power of 6411.7 W kg^{-1}. This rate capability can be ascribed to efficient charge storage inside the porous networks of rGO. These results are comparable to other reported rGO based supercapacitor cells presented in Table 3.

4. Conclusion

In summary, graphene oxide (GO) was auspiciously synthesized using the modified Hummers method and was reduced using hydrazine to obtain reduced graphene oxide (rGO). The morphological, structural and electrochemical properties of these two materials were compared to determine the better candidate for supercapacitor electrode. The oxygen based functional groups such as the epoxide in GO was drastically reduced in the rGO resulting in the reduction of the interlayer spacing in the rGO compared to the GO. We expected the GO to give more specific capacitance because of the additional pseudocapacitance effect emanating from the oxygen-containing functional groups, however it seems that the enhancement in the conductivity observed in rGO overshowed the additional pseudocapacitive effect expected from GO. It is also worth mentioning that the method used to obtain the GO and rGO plays a significant role in the derivable capacitance from them. This is because the quantity of the oxygen containing functional groups, the

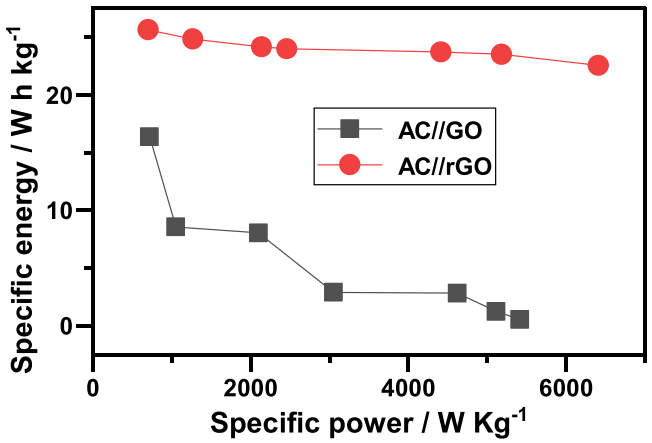

Fig. 12. Ragone plot of AC//GO and AC// rGO supercapacitor cells in 1 M KOH aqueous electrolyte and voltage window of 1.4 V.

Table 3
Electrochemical performance of some reported rGO based supercapacitor cells.

Cell components	Electrolyte	C_{sp}/ F g^{-1}	Cycle life (capacitance retention)	Specific energy/ W h kg^{-1} & corresponding specific power/ W Kg^{-1}	Ref
rGO//rGO	6 M KOH	168.5	5000 (87.5%)	5.85 & 100	[71]
PMMA/ rGO// PMMA/ rGO	1 M H_2SO_4	88	-	29.46 & 235	[72]
Alternated rGO// alternated rGO	6 M KOH	103	1000 (94%)	8.3 & 360	[73]
rGO/Co/Al LDHs// rGO/Co/ Al LDHs	6 M KOH	83.5	6000 (90%)	35.5 & 875	[74]
3D porous carbon// MnO_2/GO	1 M Na_2SO_4	84	4000 (93%)	46.7 & 100	[75]
C-WS_2 @CNFs// ACNFs	1 M KFSI/ EC-DMC	-	5500 (81.4%)	180.4 & 399.6	[76]
AC//rGO	1 M KOH	94.3	5000 (73.6%)	25.7 & 700.1	This work

number of the stacking as well as the defect density which affects the performance of the materials is a direct function of the method used in the synthesis. It has been shown that exfoliated GO perform better while rGO obtained from the exfoliated GO is more desirable.

CRediT authorship contribution statement

Nomxolisi Dywili: Methodology, Investigation, Writing. **Afroditi Ntziouni:** Data curation, Visualisation, Writing – review & editing. **Miranda M. Ndipingwi:** Investigation, Writing, Data curation, Software. **Chinwe Ikpo:** Validation, Investigation. **Assumpta C. Nwanya:** Validation, Investigation, Writing – orignal draft, Writing – review & editing, Data curation. **Konstantinos Kordatos:** Supervision, Software. **Emmanuel Iwuoha:** Conceptualization, Project administration, Resources, Funding acquisition, Supervision, Writing – review & editing.

Declaration of Competing Interest

The authors declare that they have no known competing financial interests or personal relationships that could have appeared to influence the work reported in this paper.

Acknowledgements

This work was funded through the National Research Foundation's (NRF's) South African Research Chair Initiative (SARChI) Grant No. 85102; and the Erasmus Mundus AESOP (A European and South African Partnership on Heritage and Past) Fellowship.

References

[1] Y. Wang, et al., Supercapacitor devices based on Graphene Materials.pdf, J. Phys. Chem. C. vol. 113 (2009) 13103–13107, https://doi.org/10.1021/jp902214f.
[2] S. Zheng, H. Xue, H. Pang, Supercapacitors based on metal coordination materials, Coord. Chem. Rev. (2017), https://doi.org/10.1016/j.ccr.2017.07.002.
[3] V. Ganesh, S. Pitchumani, V. Lakshminarayanan, New symmetric and asymmetric supercapacitors based on high surface area porous nickel and activated carbon, J. Power Sources vol. 158 (2006) 1523–1532.
[4] Z.S. Iro, C. Subramani, S.S. Dash, A brief review on electrode materials for supercapacitor, Int. J. Electrochem. Sci. vol. 11 (12) (2016) 10628–10643, https://doi.org/10.20964/2016.12.50.
[5] C. Portet, P.L. Taberna, P. Simon, E. Flahaut, C. Laberty-Robert, High power density electrodes for Carbon supercapacitor applications, Electrochim. Acta vol. 50 (20) (2005) 4174–4181, https://doi.org/10.1016/j.electacta.2005.01.038.
[6] P. Jampani, a Manivannan, P.N. Kumta, Advancing the supercapacitor materials and technology frontier for improving power quality, Electrochem. Soc. Interface vol. 19 (3) (2010) 57–62.
[7] Y. Shao, H. Wang, Q. Zhang, Y. Li, High-performance flexible asymmetric supercapacitors based on 3D porous graphene/MnO2 nanorod and graphene/Ag hybrid thin-film electrodes, J. Mater. Chem. C. vol. 1 (6) (2013) 1245, https://doi.org/10.1039/c2tc00235c.
[8] L.L. Zhang, R. Zhou, X.S. Zhao, Carbon-based materials as supercapacitor electrodes, J. Mater. Chem. vol. 38 (29) (2009) 2520–2531, https://doi.org/10.1039/c000417k.
[9] K. Kakaei, M.D. Esrafili, A. Ehsani, Graphene-based electrochemical supercapacitors, Interface Sci. Technol. (2019).
[10] M. Halper and J. Ellenbogen, Supercapacitors: A brief overview, Rep. No. MP 05W0000272, …, no. March, p. Report No. MP 05W0000272, 1–29, 2006, doi: Report No. MP 05W0000272.
[11] N. Mahmood, C. Zhang, H. Yin, Y. Hou, Graphene-based nanocomposites for energy storage and conversion in lithium batteries, supercapacitors and fuel cells, J. Mater. Chem. A vol. 2 (1) (2014) 15–32, https://doi.org/10.1039/C3TA13033A.
[12] A.C. Nwanya, et al., Electrochromic and electrochemical capacitive properties of tungsten oxide and its polyaniline nanocomposite films obtained by chemical bath deposition method, Electrochim. Acta vol. 128 (2014), https://doi.org/10.1016/j.electacta.2013.10.002.
[13] A.C. Nwanya, et al., Zea mays lea silk extract mediated synthesis of nickel oxide nanoparticles as positive electrode material for asymmetric supercabattery, J. Alloy. Compd. vol. 822 (2020), https://doi.org/10.1016/j.jallcom.2019.153581.
[14] H. Joon, et al., Maximizing volumetric energy density of all-graphene-oxide-supercapacitors and their potential applications for energy harvest, J. Power Sources vol. 346 (2017) 113–119, https://doi.org/10.1016/j.jpowsour.2017.02.040.
[15] Y. Zhu, et al., Graphene and graphene oxide: synthesis, properties, and applications, Adv. Mater. (2010), https://doi.org/10.1002/adma.201001068.
[16] L.W. Le Fevre, J. Cao, I.A. Kinloch, A.J. Forsyth, R.A.W. Dryfe, Systematic comparison of graphene materials for supercapacitor electrodes, ChemistryOpen vol. 8 (4) (2019) 418–428, https://doi.org/10.1002/open.201900004.
[17] M. Veerapandian, M.-H. Lee, K. Krishnamoorthy, K. Yun, Synthesis, characterization and electrochemical properties of functionalized graphene oxide, Carbon N. Y vol. 50 (11) (2012) 4228–4238, https://doi.org/10.1016/j.carbon.2012.05.004.
[18] Y. Huang, J. Liang, Y. Chen, An overview of the applications of graphene-based materials in supercapacitors, Small vol. 8 (12) (2012) 1805–1834, https://doi.org/10.1002/smll.201102635.
[19] F. Del Giudice, A.Q. Shen, ScienceDirect shear rheology of graphene oxide dispersions, Curr. Opin. Chem. Eng. vol. 16 (2017) 23–30, https://doi.org/10.1016/j.coche.2017.04.003.
[20] S.N. Alam, N. Sharma, L. Kumar, Synthesis of graphene oxide (GO) by modified hummers method and its thermal reduction to obtain reduced graphene oxide (rGO), Graphene vol. 06 (01) (2017) 1–18, https://doi.org/10.4236/graphene.2017.61001.
[21] G. Darabdhara, B. Sharma, M.R. Das, R. Boukherroub, S. Szunerits, Sensors and actuators B: chemical Cu-Ag bimetallic nanoparticles on reduced graphene oxide nanosheets as peroxidase mimic for glucose and ascorbic acid detection, Sens. Actuators B. Chem. vol. 238 (2017) 842–851, https://doi.org/10.1016/j.snb.2016.07.106.
[22] X. Zhang, D. Zhang, Y. Chen, X. Sun, Y. Ma, Electrochemical reduction of graphene oxide films: preparation, characterization and their electrochemical properties, Chin. Sci. Bull. vol. 57 (23) (2012) 3045–3050, https://doi.org/10.1007/s11434-012-5256-2.
[23] A.H. Lima, J.P. Mendonça, M. Duarte, F. Stavale, C. Legnani, G.S.G. De Carvalho, Reduced graphene oxide prepared at low temperature thermal treatment as

transparent conductors for organic electronic applications, Org. Electron. vol. 49 (2017) 165–173, https://doi.org/10.1016/j.orgel.2017.05.054.
[24] J. Yang, S. Gunasekaran, Electrochemically reduced graphene oxide sheets for use in high performance supercapacitors, Carbon N. Y vol. 51 (1) (2013) 36–44, https://doi.org/10.1016/j.carbon.2012.08.003.
[25] V. Georgakilas, et al., Functionalization of graphene: covalent and non-covalent approaches, derivatives and applications, Chem. Rev. vol. 112 (11) (2012) 6156–6214, https://doi.org/10.1021/cr3000412.
[26] P. Karthika, Functionalized exfoliated graphene oxide as supercapacitor electrodes, Soft Nanosci. Lett. vol. 02 (October) (2012) 59–66, https://doi.org/10.4236/snl.2012.24011.
[27] G. Shao, Y. Lu, F. Wu, C. Yang, F. Zeng, Q. Wu, Graphene oxide: the mechanisms of oxidation and exfoliation, J. Mater. Sci. vol. 47 (10) (2012) 4400–4409, https://doi.org/10.1007/s10853-012-6294-5.
[28] T. Aytug, et al., Vacuum-assisted low-temperature synthesis of reduced graphene oxide thin-film electrodes for high-performance transparent and flexible all-solid-state supercapacitors, ACS Appl. Mater. Interfaces vol. 10 (13) (2018) 11008–11017, https://doi.org/10.1021/acsami.8b01938.
[29] L. Lu, L. Peng, C. Zhan, W. You, S. Xiao, Enhanced electrochemical energy storage performance of reduced graphene oxide by incorporating oxygen-rich in-plane pores, J. Mater. Chem. A vol. 2 (6) (2014) 1802–1808, https://doi.org/10.1039/c3ta13678g.
[30] W. Gao, The chemistry of graphene oxide, graphene oxide reduct, Recipes, Spectrosc. Appl. (2015) 61–95, https://doi.org/10.1007/978-3-319-15500-5_3.
[31] B. Xu, et al., What is the choice for supercapacitors: graphene or graphene oxide? Energy Environ. Sci. vol. 4 (8) (2011) 2826–2830, https://doi.org/10.1039/c1ee01198g.
[32] S. Rai, R. Bhujel, B.P. Swain, Electrochemical analysis of graphene oxide and reduced graphene oxide for super capacitor applications, Proc. Int. Conf. 2018 IEEE Electron Device Kolkata Conf. EDKCON 2018 (2018) 489–492, https://doi.org/10.1109/EDKCON.2018.8770433.
[33] L. Yang, L. Zhang, X. Jiao, Y. Qiu, W. Xu, The electrochemical performance of reduced graphene oxide prepared from different types of natural graphites, RSC Adv. vol. 11 (7) (2021) 4042–4052, https://doi.org/10.1039/d0ra09684a.
[34] N.R. Dywili, et al., Graphene oxide decorated nanometal-poly(anilino-dodecylbenzene sulfonic acid) for application in high performance supercapacitors, Micromachines vol. 10 (2) (2019) 1–17, https://doi.org/10.3390/mi10020115.
[35] S. Park, J. An, J.R. Potts, A. Velamakanni, S. Murali, R.S. Ruoff, Hydrazine-reduction of graphite- and graphene oxide, Carbon N. Y vol. 49 (9) (2011) 3019–3023, https://doi.org/10.1016/j.carbon.2011.02.071.
[36] D. Konios, M.M. Stylianakis, E. Stratakis, E. Kymakis, Dispersion behaviour of graphene oxide and reduced graphene oxide, J. Colloid Interface Sci. vol. 430 (2014) 108–112, https://doi.org/10.1016/j.jcis.2014.05.033.
[37] J. Song, X. Wang, C.-T. Chang, J. Song, X. Wang, C.-T. Chang, Preparation and characterization of graphene oxide, J. Nanomater. vol. 2014 (2014) 1–6, https://doi.org/10.1155/2014/276143.
[38] X. Jiao, Y. Qiu, L. Zhang, X. Zhang, Comparison of the characteristic properties of reduced graphene oxides synthesized from natural graphites with different graphitization degrees, RSC Adv. vol. 7 (82) (2017) 52337–52344, https://doi.org/10.1039/c7ra10809e.
[39] S.J. Mu, Y.C. Su, L.H. Xiao, S.D. Liu, T. Hu, H.B. Tang, X-ray difraction pattern of graphite oxide, Chin. Phys. Lett. vol. 30 (9) (2013) 10–13, https://doi.org/10.1088/0256-307X/30/9/096101.
[40] M. Møller, R.E. Johnsen, P. Norby, In situ X-ray powder diffraction studies of the synthesis of graphene oxide and formation of reduced graphene oxide, J. Solid State Chem. vol. 240 (2016) 49–54, https://doi.org/10.1016/j.jssc.2016.05.019.
[41] N. Njomo, et al., Graphenated tantalum(IV) oxide and poly(4-styrene sulphonic acid)-doped polyaniline nanocomposite as cathode material in an electrochemical capacitor, Electrochim. Acta vol. 128 (2014) 226–237, https://doi.org/10.1016/j.electacta.2013.12.150.
[42] L. Shahriary, A.A. Athawale, Graphene oxide synthesized by using modified hummers approach, Int. J. Renew. Energy Environ. Eng. vol. 02 (01) (2014) 58–63.
[43] L. Wan, C. Du, S. Yang, Synthesis of graphene oxide / polybenzoxazine-based nitrogen-containing porous carbon nanocomposite for enhanced supercapacitor properties, Electrochim. Acta (2017), https://doi.org/10.1016/j.electacta.2017.08.086.
[44] T.-T. Wu, Preparation and characteristics of graphene oxide and its thin films, Surf. Coat. Technol. vol. 231 (2013) 487–491, https://doi.org/10.1016/j.surfcoat.2012.05.066.
[45] C. Sarkar, S.K. Dolui, Synthesis of copper oxide/reduced graphene oxide nanocomposite and its enhanced catalytic activity towards reduction of 4-nitrophenol, RSC Adv. vol. 5 (75) (2015) 60763–60769, https://doi.org/10.1039/c5ra10551j.
[46] R.K. Prud, I. a Aksay, R. Car, Raman spectra of graphite oxide and functionalized graphene sheets, no. Fig. 1, Nano (2008) 1–6, https://doi.org/10.1021/nl071822y.
[47] I. Childres, L. Jauregui, W. Park, H. Cao, Y. Chen, Raman spectroscopy of graphene and related materials, N. Dev. Phot. Mater. Res. (2013) 1–20, https://doi.org/10.1016/B978-0-444-53175-9.00016-7.
[48] G.K. Yogesh, E.P. Shuaib, P. Roopmani, M.B. Gumpu, U.M. Krishnan, D. Sastikumar, Synthesis, characterization and bioimaging application of laser-ablated graphene-oxide nanoparticles (nGOs), Diam. Relat. Mater. (2020), https://doi.org/10.1016/j.diamond.2020.107733.
[49] A.C. Ferrari, Raman spectroscopy of graphene and graphite: disorder, electron-phonon coupling, doping and nonadiabatic effects, Solid State Commun. vol. 143 (1–2) (2007) 47–57, https://doi.org/10.1016/j.ssc.2007.03.052.
[50] Q.A. Khan, A. Shaur, T.A. Khan, Y.F. Joya, M.S. Awan, Characterization of reduced graphene oxide produced through a modified Hoffman method, Cogent Chem. vol. 3 (1) (2017), https://doi.org/10.1080/23312009.2017.1298980.
[51] H.S. Wahab, S. Ali, A. Abdul Hussein, S.H. Ali, and A.M. Abdul Hussein, Synthesis and Characterization of Graphene by Raman Spectroscopy, 2015.
[52] S. Stankovich, et al., Synthesis of graphene-based nanosheets via chemical reduction of exfoliated graphite oxide, Carbon N. Y vol. 45 (7) (2007) 1558–1565, https://doi.org/10.1016/j.carbon.2007.02.034.
[53] S. Drewniak, R. Muzyka, A. Stolarczyk, T. Pustelny, M. Kotyczka-Morańska, M. Setkiewicz, Studies of reduced graphene oxide and graphite oxide in the aspect of their possible application in gas sensors, Sensors vol. 16 (1) (2016) 103, https://doi.org/10.3390/s16010103.
[54] M. Hashemi, et al., Layer-by-layer assembly of graphene oxide on thermosensitive liposomes for photo-chemotherapy, Acta Biomater. vol. 65 (2018) 376–392, https://doi.org/10.1016/j.actbio.2017.10.040.
[55] M.S. Amir Faiz, C.A. Che Azurahanim, S.A. Raba'ah, M.Z. Ruzniza, Low cost and green approach in the reduction of graphene oxide (GO) using palm oil leaves extract for potential in industrial applications, Results Phys. (2020), https://doi.org/10.1016/j.rinp.2020.102954.
[56] Y. Li, H. Li, A. Du, M. Wang, J. Zeng, Morphology and isothermal crystallization of graphene oxide reinforced biodegradable poly (butylene succinate), Polym. Testing vol. 59 (2017) 1–9, https://doi.org/10.1016/j.polymertesting.2017.01.014.
[57] S. Gilje, et al., Processable aqueous dispersions of graphene nanosheets, Nat. Nanotechnol. vol. 3 (2) (2008) 101–105, https://doi.org/10.1038/nnano.2007.451.
[58] B. Faust, Ultraviolet/visible spectroscopy, Mod. Chem. Tech. vol. 3 (1) (1997) 92–115, https://doi.org/10.1002/chin.200521298.
[59] Q. Lai, et al., Ultraviolet-visible spectroscopy of graphene oxides, AIP Adv. vol. 032146 (2012) 3–8, 10.1063/1.4747817.
[60] Q. Lai et al., Ultraviolet-visible spectroscopy of graphene oxides, vol. 032146, no. 2012, pp. 3–8, 2012, doi: 10.1063/1.4747817.
[61] R. Udayabhaskar, R.V. Mangalaraja, T. Pandiyarajan, B. Karthikeyan, D. Contreras, Spectroscopic investigation on graphene-copper nanocomposites with strong UV emission and high catalytic activity, Carbon vol. 124 (2017) 256–262, https://doi.org/10.1016/j.carbon.2017.08.061.
[62] S.K. Bhunia, N.R. Jana, Reduced graphene oxide-silver nanoparticle composite as visible light photocatalyst for degradation of colorless endocrine disruptors, ACS Appl. Mater. Interfaces vol. 6 (22) (2014) 20085–20092, https://doi.org/10.1021/am505677x.
[63] D. Jariwala, A. Srivastava, P.M. Ajayan, Graphene synthesis and band gap opening, J. Nanosci. Nanotechnol. vol. 11 (8) (2011) 6621–6641, https://doi.org/10.1166/jnn.2011.5001.
[64] N.A. Devi, S. Sinha, W.I. Singh, S. Nongthombam, B.P. Swain, Silver-decorated reduced graphene oxide nanocomposite for supercapacitor electrode application, Bull. Mater. Sci. (2022), https://doi.org/10.1007/s12034-021-02583-3.
[65] J. Zhu, J. Zu, J. Liu, Y. Wang, M. Pei, Y. Xu, Self-assembled reduced graphene oxide films with different thicknesses as high performance supercapacitor electrodes, J. Energy Storage (2020), https://doi.org/10.1016/j.est.2020.101795.
[66] B. Rajagopalan, J.S. Chung, Reduced chemically modified graphene oxide for supercapacitor electrode, Nanoscale Res. Lett. (2014), https://doi.org/10.1186/1556-276X-9-535.
[67] S. Bera, M. Miah, T.K. Mondal, A. Debnath, S.K. Saha, Electrochimica acta synthesis of new mixed metal oxide RuNi 2 O 4 phase decorated on reduced graphene oxide for supercapacitor applications, Electrochim. Acta vol. 424 (March) (2022), 140666, https://doi.org/10.1016/j.electacta.2022.140666.
[68] P.K. Jha, S.K. Singh, V. Kumar, S. Rana, S. Kurungot, N. Ballav, High-level supercapacitive performance of chemically reduced graphene oxide, Chem (2017), https://doi.org/10.1016/j.chempr.2017.08.011.
[69] M.M. Ndipingwi, et al., Engineering the chemical environment of lithium manganese silicate by Mn ion substitution to boost the charge storage capacity for application in high efficiency supercapattery, Electrochim. Acta (2022), https://doi.org/10.1016/j.electacta.2022.140180.
[70] D. Prakash, S. Manivannan, N, B co-doped and crumpled graphene oxide pseudocapacitive electrode for high energy supercapacitor, Surf. Interfaces (2021), https://doi.org/10.1016/j.surfin.2021.101025.
[71] B.J. Choudhury, K. Ingtipi, V.S. Moholkar, Improved energy density of reduced graphene oxide based aqueous symmetric supercapacitors in redox-active and ' water-in-salt ' electrolytes, J. Energy Storage vol. 52 (PC) (2022), 105006, https://doi.org/10.1016/j.est.2022.105006.
[72] G. Sahoo, N. Sarkar, D. Sahu, S.K. Swain, Nano gold decorated reduced graphene oxide wrapped polymethylmethacrylate for supercapacitor applications, RSC Adv. (2017), https://doi.org/10.1039/c6ra26930c.
[73] J. Yoo, M.S. Tahir, I. Rabani, Y. Seo, Applied Surface Science Fabrication of multilayer film with graphene oxide of different surface charge through electrospray deposition, Appl. Surf. Sci. vol. 599 (March) (2022), 153977, https://doi.org/10.1016/j.apsusc.2022.153977.
[74] W. Zhang, et al., Asymmetric electrochemical capacitors with high energy and power density based on graphene/CoAl-LDH and activated carbon electrodes, RSC Adv. (2013), https://doi.org/10.1039/c2ra23283a.
[75] Y. Zhao, et al., High-performance asymmetric supercapacitors based on multilayer mno2/graphene oxide nanoflakes and hierarchical porous carbon with enhanced cycling stability, Small (2015), https://doi.org/10.1002/smll.201401922.
[76] W. Gao, The chemistry of graphene oxide, Graph. Oxide Reduct. Recipes Spectrosc. Appl. (2015) 61–95.